Nematic ordering in porous glasses: A deuterium NMR study

S. Kralj,[1] A. Zidanšek,[1] G. Lahajnar,[1] I. Muševič,[1] S. Žumer,[1,2] R. Blinc,[1,2] and M. M. Pintar[3]
[1]*J. Stefan Institute, University of Ljubljana, Jamova 39, 61111 Ljubljana, Slovenia*
[2]*Department of Physics, University of Ljubljana, Jadranska 19, 61111 Ljubljana, Slovenia*
[3]*Department of Physics, University of Waterloo, Waterloo, Ontario, Canada N2L 3G1*
(Received 4 October 1995)

A deuterium NMR study of the pentylcyanobiphenyl liquid crystal confined to a controlled pore glass matrix with pore radii of 12, 150, and 200 nm was performed. In the 12-nm sample the nematic to isotropic transition is gradual. In the nematic phase the absorption spectrum is substantially narrowed due to translational diffusion of nematic molecules, which is effective because of the inhomogeneous nematic ordering. The external magnetic field influence is negligible. The onset of nematic ordering is bulklike in the 150- and 200-nm samples. There, the absorption spectrum is strongly affected by the external magnetic field. The 150-nm sample exhibits memory effects depending on history of temperature and external field changes.

PACS number(s): 64.70.Md, 76.60.−k

I. INTRODUCTION

The behavior of liquid crystals (LCs) confined to various geometries is a field of great interest for years. The reason behind this lies in the richness [1] of physical phenomena that liquid crystals exhibit and their susceptibility to geometry and the typical size of the confining cavity, and their interaction with it. The early works mostly treated LCs confined to spherical [2–5] or cylindrical [6–10] cavities.

More recently the interest has shifted to LCs immersed in various porous matrices [11], which provide a more complex confining geometry. In these systems the average characteristic void pore size is below 1 μm, the voids are strongly interconnected, and the pores' geometry is in some cases quite irregular. In addition to finite size and surface effects, which have been extensively studied in regular geometries, this introduces into the system also a kind of randomness.

Typical examples of such host matrices are controlled porous glass (CPG) [12], Vycor glass [13,14], and aerogels [15–19]; the inherent randomness imposed by geometry is largest in aerogels and lowest in CPG. The controlled porous glass consists of a strongly connected network of curved cylindrically shaped pores with a relatively narrow distribution of radia sizes. The Vycor glass has similar geometrical characteristics with the exception that local deviations from the cylindrical geometry are larger. In the case of aerogels the voids are of rather irregular shape and even more strongly interconnected.

Different experimental techniques (deuterium NMR [18,19,13], light scattering [15,20–22], x rays [16], precision calorimetry [15,17], and time-resolved grating optical Kerr effect experiments [23]) have led essentially to the same conclusion that the behavior of LCs immersed in porous matrices strongly depends on the mean characteristic pores' void size, its shape, the interconnectedness of voids, as well as the anchoring and wetting properties of the internal surface. The following general characteristics have been observed. (i) The bulk transition temperature T_{NI} could be shifted either upward or downward by several degrees. The direction of the phase transition temperature shift ΔT_{NI} depends on the size of the cavity and on the ordering properties of the cavity surface. (ii) For a cavity size much smaller than a micrometer the first-order bulk nematic to isotropic (N-I) phase transition is replaced by a gradual evolution of the nematic order. (iii) In many cases the surface induced paranematic order is observed in the isotropic phase. This ordering is a result of strong surface interactions and persists far into the isotropic phase.

Despite numerous studies the understanding of these systems is still incomplete. Most theoretical descriptions are based on the Landau–de Gennes approaches [19,13,24]. For example, a model of independent pore segments was used [13] for a nematic liquid crystal confined in Vycor glass with rather well defined pores. Some studies explore the analogies between the nematic liquid crystals in pores and the random magnetic systems [24,25], despite the different basic symmetries of these systems. Maritan *et al.* [25] proposed that the main qualitative properties of a nematic liquid crystal confined in a randomly interconnected porous matrix are similar to a magnetic system in a random external field. Cleaver *et al.* [24] analyzed the behavior of confined nematic liquid crystals in analogy with the random anisotropy magnetic system. It should be stressed that the above mentioned models only partially explain the phase behavior of confined nematic liquid crystals. More detailed experimental results are needed to test further the models proposed so far.

Dadmun and Muthukumar [12] have studied the effect of the confinement on *p*-azoxyanisole liquid crystals in controlled pore glasses by differential scanning calorimetry. The mean pore radii of their samples were $R \approx 156$,

17, and 8-nm, respectively. They showed that the surface anchoring effects are dominant in the 156-nm sample ($\Delta T_{NI} > 0$) whereas the finite size effects prevail in the two smaller samples ($\Delta T_{NI} < 0$).

Here we report a deuterium NMR absorption study of the nematic liquid crystal pentylcyanobiphenyl (5CB) confined in a CPG matrix of various pore sizes. The research is a continuation of our earlier deuterium NMR study of nematic liquid crystals confined to aerogel matrices [18,19]. The paper is organized as follows. In Sec. II the sample and the experimental procedures are described. The theoretical background is given in Sec. III. Experimental results are presented in Sec. IV. In Sec. V the results are discussed and the conclusions are given in Sec. VI.

II. SAMPLE AND EXPERIMENTAL SETUP

In order to clarify the size, shape, surface roughness, and interconnectedness of the host matrix, atomic force microscopy (AFM) and scanning electron microscopy (SEM) were used. The results are shown in Figs. 1(a)–1(d). From the SEM pictures [Figs. 1(a) and 1(b)] we can clearly see that the cavities are of the cylindrical form and strongly interconnected. The cylindrical cavities are curved and the curvature radii are of the order of several pore diameters. The AFM measurements [Figs. 1(c) and 1(d)] reveal that the CPG grain surfaces are smooth even on the nanometer scale, with no preferred direction within the surface plane. The grain surface is nonfractal. Note that the AFM pictures show the external surface of

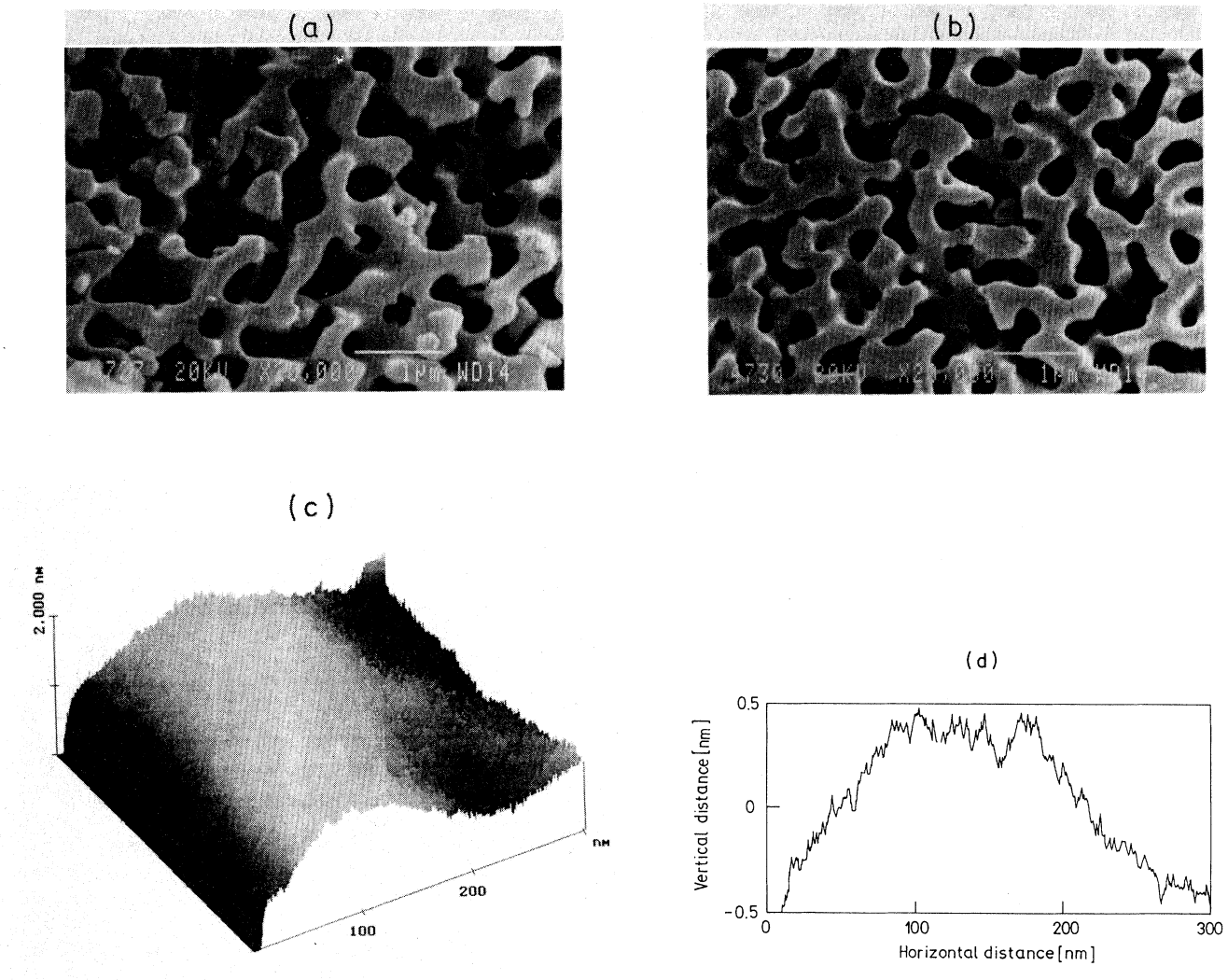

FIG. 1. (a) and (b) SEM and (c) and (d) AFM images. The CPG samples with pore radii (a) $R \approx 200$ nm and (b) $R \approx 150$ nm are shown. Note that in all cases the outer surface of the CPG matrices was probed. The 3D AFM image of the CPG ($R \approx 150$ nm) surface is presented in (c) and the surface profile is shown in (d).

the CPG grains, which we believe is similar to the pores' inner surfaces.

We can thus loosely describe the host CPG matrix as a system of randomly interconnected cylindrical pores of radius R. In the experiment we have used CPG matrices with the cylinder radii of 12, 150, and 200-nm, respectively. In the following these samples will be designated as 12-, 150-, and 200-nm samples.

The pores of a CPG sample were filled with the 5CB liquid crystal in the isotropic phase by capillary action. The liquid crystal was deuterated at the βd_2 position. Deuteron NMR spectra were recorded at a resonance frequency of 58.37 MHz in a 9-T superconducting magnet. A $(\pi/2)_x$-$(\pi/2)_y$ pulse sequence with phase cycling was used to obtain the spectra.

III. THEORETICAL BACKGROUND

A. Free energy

The isotropic to nematic phase transition in CPG will be analyzed within the Landau–de Gennes theory [26]. The nematic ordering within cavities is described with a nematic director field $\vec{n}(r)$ and a nematic orientational order parameter $S(\vec{r})$. Whereas the nematic director determines the direction of the local average of the long axis of nematic molecules, $S(\vec{r})$ describes the amount of nematic order around $\vec{n}(r)$. In this description we neglect the biaxiality effects. The free energy F is [26]

$$F = \int \Big(a(T-T_*)S^2 - bS^3 + cS^4 + L(\nabla S)^2 + \frac{K_1}{2}(\nabla\cdot\vec{n})^2 + \frac{K_2}{2}[\vec{n}\cdot(\nabla\times\vec{n})]^2 + \frac{K_3}{2}(\vec{n}\times\nabla\times\vec{n})^2 + K_{13}\nabla(\vec{n}\cdot\nabla\vec{n}) - \frac{K_{24}}{2}\nabla(\vec{n}\cdot\nabla\vec{n}+\vec{n}\times\nabla\vec{n})\Big) - \frac{\Delta\chi S B^2}{2\mu_0}\frac{3(\vec{n}\cdot\vec{e}_f)^2-1}{2}dV - \int W_0 g(\vec{n},S)dA. \quad (1)$$

In the above expression, a, b, c, and T_* are the material constants L and K_i ($i = 1, 2, 3, 13, 24$) are the elastic constants. The external magnetic field $\vec{B} = B\vec{e}_f$ is applied along the direction $\vec{e}_f$ and $\Delta\chi$ is the anisotropy of the diamagnetic susceptibility. The constant W_0 measures the anchoring [27] or wetting [28] strength. The dimensionless function $g(\vec{n}, S)$ describes the S and $\vec{n}$ dependence of the surface free energy. The director dependent part of $g(\vec{n}, S)$ is conventionally expressed [29,30] as $g(\vec{n}, S) = S(\vec{e}_s\cdot\vec{n})^2$, where the unit vector $\vec{e}_s$ describes the local easy axis of the surface. This unit vector points in the direction that minimizes the anisotropic part of the surface anchoring potential.

The set of elastic constants L, K_i, i = 1–24, is the smallest set [26,31,32] that is necessary for a qualitative description of the experimental results. The constants K_{13} and K_{24} are the so-called divergence or surface elastic constants [33]. Mathematically, the terms related to these constants can be transformed to the surface terms by transforming the volume integral into the integral over the surface enclosing the nematic phase. The divergence constants are, in the lowest order, linear [31,34,35] in S. In contrast, the bulk Frank elastic constants ($i = 1, 2, 3$) are to a good approximation proportional to S^2. The constant L is temperature independent. In this discussion we will assume that all bulk elastic constants are equal: $K_1/S^2 = K_2/S^2 = K_3/S^2 = L \equiv K$.

The orientational ordering $\vec{n}(\vec{r})$ of a nematic LC's confined to a cavity of typical radius R depends on the relative strength of the surface anchoring, as well as on the elastic and external field forces. In order to estimate the relative importance of these effects we introduce [36] the external magnetic field coherence length $\xi_f = \sqrt{\mu_0 KS/(\Delta\chi B^2)}$, the surface extrapolation length $d_e = KS/W_0$, and the nematic coherence length $\xi_n(T = T_{NI}) = 1\sqrt{a}(T_{NI} - T_*)/K$, which is defined at the temperature $T = T_{NI}$ of the bulk sample. The relative strength [36] of the surface versus elastic forces is estimated by the ratio R/d_e. Similarly, the relative strength of the external magnetic field versus elastic forces is given by R/ξ_f.

In the case $R/\xi_f \gg 1$ the external magnetic field effects are dominant and tend to align $\vec{n}$ along $\vec{e}_f$. In the regime $R/\xi_f \ll 1$ the magnetic field effects are negligible. Similarly, in the case $R/d_e \gg 1$ the surface interaction fixes $\vec{n}$ along $\vec{e}_s$, which is the so-called [27] strong anchoring regime. In the weak anchoring regime ($R/d_e \sim 1$) the orientation of $\vec{n}$ at the surface is not merely dictated by the surface, but depends also on the nematic director field far from the surface.

B. Deuterium NMR absorption spectra

The nematic ordering within a submicrometer cavity can be determined well using deuterium NMR. In the absence of motional averaging, a deuterated nematic molecule (positioned at $\vec{r}$ in the pore) contributes two sharp lines to the NMR absorption spectrum. The two lines are separated by [37] $\Delta\nu$:

$$\Delta\nu(\vec{r}) = \frac{S(\vec{r})}{S_b}\frac{\Delta\nu_b}{2}[3\cos^2\theta_B(\vec{r}) - 1]. \quad (2)$$

Here θ_B denotes the angle between the external magnetic field $\vec{B}$ and the nematic director $\vec{n}(\vec{r})$, S_b represents the bulk nematic orientational order parameter, and $\Delta\nu_b$ is the NMR absorption line splitting of the bulk nematic phase.

When the effects of the external magnetic field on the director profile are negligible, there is no preferred direction within our CPG samples. If we assume $S(\vec{\mathbf{r}}) \simeq S_b$ and there is no motional narrowing of the absorption spectrum $I(V)$, the whole sample is expected to exhibit a powder line shape of width $\Delta\nu_b$. For stronger magnetic fields ($R/\xi_f \sim 1$) there is a preferred direction, which is reflected in the outer parts of the spectrum that become more pronounced. In the limit $R/\xi_f \gg 1$ all molecules tend to be aligned along $\vec{e}_f$ and the spectrum consist of two lines separated by $\Delta\nu_b$.

In the case of nonhomogeneous nematic ordering the motional narrowing can strongly affect the absorption spectrum. The motional narrowing is pronounced if the changes of the nematic ordering are significant over a distance $d_D \approx \sqrt{D/\Delta\nu_b}$ that a molecule diffuses during the NMR observation [37,38]. In the nematic phase of the 5CB liquid crystal the average translational diffusion constant D is about 10^{-11} $m^2 s^{-1}$ and the line splitting is $\Delta\nu_b \approx 40$ kHz, which gives $d_D \approx 15$ nm.

In the isotropic phase $S(\vec{r}) = 0$ and consequently the absorption spectrum consists of a single line. But recent experiments on similar systems [39] suggest that in the isotropic phase the pores' surface is wetted with a weakly developed paranematic layer of thickness comparable to the length of the nematic molecule. In addition, molecules reside for a relatively long time at the surface due to strong surface interactions. In the case that the anisotropic part of the surface interaction enforces only one direction in space and has a relatively large surface to volume ratio the surface paranematic layer results in the splitting of $I(\nu)$ in the isotropic phase [39]. If the surface normal changes significantly over a distance d_D, which is the case, in our CPG samples, the influence of the surface layer on $I(\nu)$ is weaker. In this case, in addition to the averaging over $S(\vec{r})$ values that the molecules experience during the measurement, also averaging over orientations that molecules take in the surface layer over a linear distance d_D is realized.

IV. EXPERIMENTAL DATA

The temperature variation of the width of the deuterium spectrum for all the samples as well as of the bulk half-splitting is shown in Fig. 2. The corresponding line shape evolution from a single line to a broad line with two well defined peaks is depicted in Figs. 3–5.

The spectrum evolution of the 12-nm sample (Fig. 3) appears to be gradual and $\Delta\nu$ reaches approximately $2/3\Delta\nu_b$ in the nematic phase. In the 150-nm (Fig. 4) and 200-nm samples (Fig. 5) the linewidth in the isotropic phase is within the experimental error, equal to that of the bulk sample. Here the onset of the nematic phase

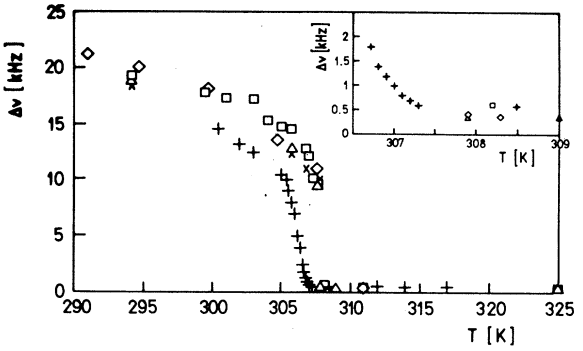

FIG. 2. Temperature evolution of the absorption spectrum width of the 12-nm (+), 150-nm (□, path *b*; ×, path *a*), 200-nm (△), and the bulk (◇) sample. The half-height widths are shown for the 12- and 150-nm samples (measured via path *b*) and the isotropic phase of all samples. The spectral half splittings are shown for the 150-nm (measured via path *a*), 200-nm, and bulk samples in the nematic phase. Paths *a* and *b* are schematically shown in Fig. 4. The inset shows the details close to T_{NI}.

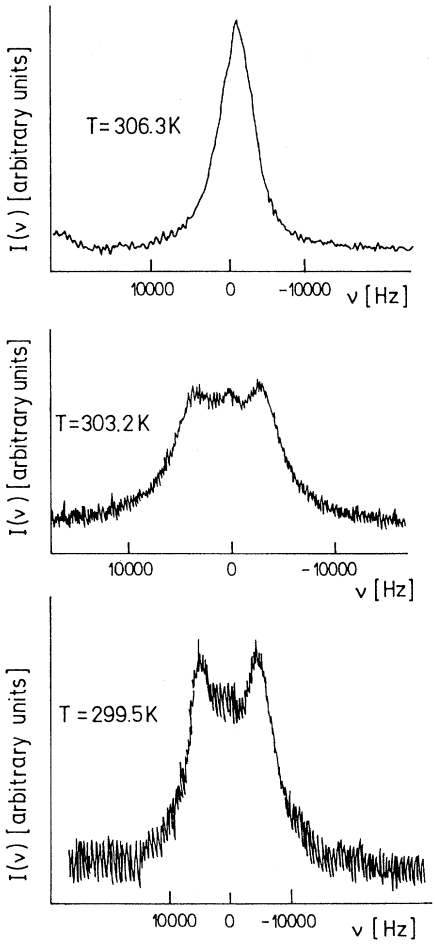

FIG. 3. Temperature evolution of the absorption spectra of the 12-nm sample in the nematic phase.

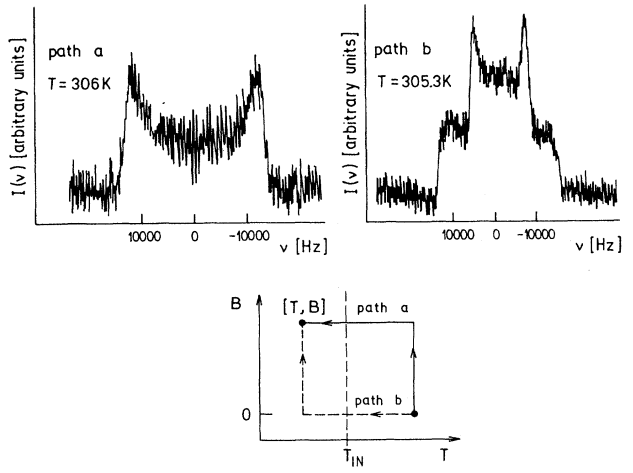

FIG. 4. Typical absorption spectra of the 150-nm sample in the nematic phase reached via different paths given at the bottom of the figure.

is discontinuous with a negligible shift of the transition temperature in comparison to the bulk nematic-isotropic transition. As can be seen from Figs. 4 and 5, the external magnetic field strongly influences the absorption spectrum, particularly in the 200-nm sample. The line splitting $\Delta\nu$ is, in the 150-nm and 200-nm samples narrower yet comparable to the bulk splitting $\Delta\nu_b$ at all temperatures. We have also observed the hysteresis in the 150-nm sample by measuring the "zero field cooled" and "field cooled" line shapes. Two different paths were used (see the inset to Fig. 4): (a) the sample was cooled from the isotropic phase into the nematic phase at a constant value of $B \approx 9$ T (path a), and (b) the sample was cooled from the isotropic phase into the nematic phase in zero field and then the sample was put into the magnetic field for measurements (path b).

V. DISCUSSION

In order to explain the observed temperature dependence of the spectrum in the N-I transition region and deep in the nematic phase one has to know at least a qualitative profile of the director field in an average domain. We shall describe a typical pore section in our sample with a long curved cylinder of radius R. The sample can thus be viewed as an ensemble of strongly interconnected cylindrical segments. In the following such a segment will be called a domain.

Let us first discuss the situation when the external field influence is negliglible (i.e., $R/\xi_f \ll 1$). In this case the director field is determined only by elastic and surface interactions. The AFM measurments reveal that the segment surface is smooth on the correlation length scale. This suggests planar anchoring conditions if the steric surface interaction contribution is dominant. This belief is based on recent experiments [40] on differently treated surfaces, which indicate that the orientation of LCs at the surface is often dominantly governed by steric effects. Adopting this assumption, we expect the nematic director field to run along the local orientation of the segment's long axis. We name such a nematic pattern the axial structure. At the joints of segments, in general, the director field cannot be topologically resolved without forming defects [12,41] (see Fig. 6). We assume that the concentration of defects is roughly given by the concentration of joints.

Because no direction in the sample is preferred, the distribution of nematic director orientations is isotropic. However, if $R/\xi_f \approx 1$ or is even larger, then the field influence is important, partially orienting the director field in its direction. In our measurements the field correlation length is $\xi_f \approx 0.5$ μm. Thus the condition $R/\xi_f \ll 1$ is realized only in the 12-nm sample.

A. The N-I transition

The experiment reveals that in the 12-nm sample the N-I transition is gradual and shifted towards lower tem-

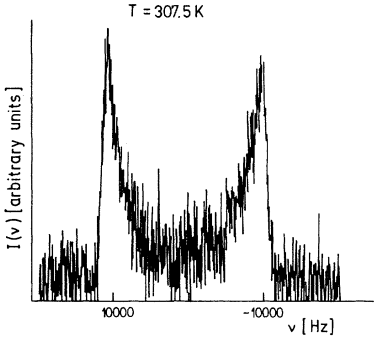

FIG. 5. Typical absorption spectrum of the 200-nm sample measured in the nematic phase.

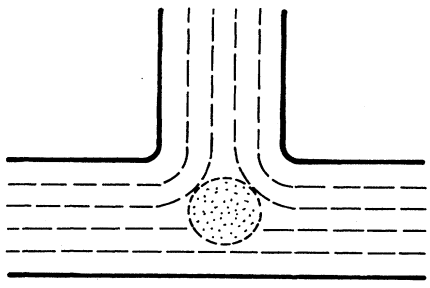

FIG. 6. Schematic presentation of the nematic director field at the intersection of two domains. The dotted region indicates the core of the defect.

peratures in comparision to the bulk behavior. In contrast in the 150- and 200-nm samples the cylinders are large enough to allow for a bulklike discontinuous N-I transition with a negligible shift of the transition temperature.

To explain the gradual onset of nematic ordering in the 12-nm sample we first briefly review the effects of confinement on the character of the N-I phase transition for a general geometry of the confining cavity. In bulk the nematic to isotropic (N-I) phase transition is discontinuous because of symmetry reasons. The confinement can affect the nature of this transition. For example, it can shift the transition temperature or even cause a gradual growth of the nematic order upon cooling from the isotropic phase. A qualitative change of the character of the phase transition can be caused by the surface ordering potential [19,13,30,42], and the influence of strong elastic deformations [24,42,43]. The onset of these phenomena is closely connected to the critical cavity size R_c.

1. *Surface ordering potential*

Let us assume that the smooth surface introduces a local ordering field that is, in the lowest order, linear in the nematic orientational order parameter. For the surface potential $g(S,\vec{n}) = S$ [30], the critical cavity size R_c is approximately [19]

$$R_c \approx 16c^2 W_0/b^3. \tag{3}$$

For $R > R_c$ we have a bulklike, discontinuous N-I transition, whereas for $R < R_c$ the theory predicts a gradual growth of the nematic ordering. For a 5CB liquid crystal the critical size is $R_c \approx 10^{-4} W_0$ m^2/N. By taking $W_0 \approx 10^{-6}$–10^{-3} J/m^2, one gets, for the upper limit, $R_c \approx 100$ nm. This estimate is in agreement with the experimental results by Yokoyama [44], who observed a continuous onset of nematic ordering for 5CB confined between rubbed poly(vinyl alcohol) walls separated by 83 nm.

We now discuss whether this effect could be responsible for the observed gradual nematic temperature evolution in the 12-nm CPG sample. Recent experimental results [13,23,12,39] in similar samples suggest that the surface interaction within a pore tends to increase the nematic ordering. This is usually manifested in the isotropic phase where the opposing tendency of the surface roughness or curvature is less effective because of the shorter nematic correlation length. According to Eq. (3), the surface ordering tendency is relevant in the 12-nm sample if $W_0 \sim 10^{-4}$ J/m^2, which is a reasonable anchoring strength. But if this surface anchoring is dominant, it will also shift upward the temperature regime where the nematic ordering becomes apparent. However, in our experiment the phase transition temperature was shifted downward for approximately 1 K. This could be explained by considering the surface disordering term proportional to S^2, which is known to shift the transition towards lower temperatures [19,28,45]. Recent studies [45] suggest that this term plays an important role in porous silica surfaces. However, Dadmun and Muthukumar [12] observed that in a similar sample of relatively large radius ($R \approx 0.1$ μm) the ordering surface term is dominant. Because they have the same scaling properties [19] with respect to R we do not think that this is the case.

Note that the K_{13} and K_{24} terms are, in the lowest order, also linear [34,35] in S. In the case that this linear contribution is negative it could cause the observed change of the transition character. These contributions can be important if the director distribution is substantially different from the proposed predominantly homogeneous axial alignment. Namely, in the noncurved axial-like structure the K_{13} and K_{24} terms do not contribute. Large deviations from this alignment can be realized only at the intersections of domains or at strongly curved parts of domains.

2. *Influence of strong elastic deformations*

One distinguishes between singular and nonsingular elastic deformations. In the singular case the uniaxial director field is discontinuous (a so-called defect or disclination) [41]. The nematic liquid crystal lowers the high elastic nematic free energy at the defect size by surrounding it by a paranematic (weakly ordered nematic, i.e., essentially isotropic) core. If the defect size, which is roughly equal to ξ_n, becomes comparable to the typical system size, it causes a gradual growth of the nematic order on cooling from the isotropic phase. Numerical summations of the nematic structures confined to a spherical cavity [42,43] indicates that this effect can be important in cavities smaller than 0.1 μm.

Similar effect appears if the director field strongly, but in a nonsingular way, varies on the nematic correlation length scale. This can be achieved by a rough or strongly curved surface where the surface induced orientational tendency strongly varies from site to site. In the case that the strong director field deformations are a consequence of some "random" source this effect can be described using the random anisotropy nematic model. Cleaver *et al.* [24] have shown that strong enough randomness can suppress the discontinuity of the N-I transition.

In our 12-nm sample both effects might be important. The SEM picture reveals a relatively high concetration of domain joints, where defects most probably appear. They could cause a gradual onset of nematic ordering [42,43], at least in some regions, because the cavity size is comparable to $\xi_n(T_{NI})$. To discuss the effect of nonsingular director field deformations we first focus to AFM images. They indicate that the surface is smooth on the molecular scale. This suggests that no randomness is induced by the surface. Randomly interconnected seg-

ments also introduce randomness into the system, but on a length scale greater than R. We believe that this randomness is too dilute to change the global character of the transition of the whole sample. But the SEM pictures reveal that in some regions the curvature of cylindrical segments can be quite large on the ξ_n scale. These nonsingular deformed regions have similar effects on the local phase ordering as defects.

It is also possible that the gradual onset of the nematic ordering is the result of a superposition of local domain transitions. The main domains' characteristics generally differ (different lengths of domains, kinds of domain intersections, etc.) and consequently the N-I transition in domains can appear at different temperatures. These local transitions can be either discontinuous or gradual due to effects described above. Therefore, the overall response of the system can be virtually gradual also in the case where most of the domain transitions are discontinuous but take place at different temperatures.

B. Nematic phase

In the 12-nm sample the width of the spectrum is narrower than in the bulk sample in the whole temperature interval measured below T_{NI}. In contrast, in larger pores there is no observed narrowing. The main effects that could cause narrowing are the (i) motional narrowing, a depression of the average degree of nematic ordering, which can be realized because of either (ii) surface disordering effect or (iii) large concetration of defects.

In the following we analyze which of the effects mentioned is dominant in our case. For this purpose we define the narrowing factor $\delta(R)$ as

$$\delta(R) = 1 - \langle \Delta\nu \rangle / \Delta\nu_b. \tag{4}$$

Here $\langle \Delta\nu \rangle$ stands for the average spectrum width during the NMR observation time.

(i) The motional narrowing is effective if the nematic ordering [both director field and $S(\vec{r})$] is inhomogeneous on the scale characterized by the distance d_D [37,38]. The case of inhomogenity in $S(\vec{r})$) will be treated in connection with effects given in (ii) and (iii). Here we limit the discussion to the case where only $\vec{n}(\vec{r})$ is inhomogeneous. To analyze the motional narrowing due to the director field spatial variation we assume that $\vec{n}(\vec{r})$ is predominantly axial within domains and we neglect joints. For such a case the only source of motional narrowing can be due to the reorientation of the cylindrical segment long axis. In order to estimate this effect we assume that the cylinder axis is curved with radius $R_{\rm curv}$. We further assume that a molecule moves during the measurement time for a distance d_D along the circular path of radius $R_{\rm curv}$. Consequently,

$$\delta(R) \approx \frac{1}{2}\left(\frac{d_D}{R_{\rm curv}}\right)^2, \tag{5}$$

assuming $d_D/R_{\rm curv} < 1$. The SEM photographs reveal that in all samples the curvature of cylinders is typically $R_{\rm curv} \approx 3$–$5R$, suggesting $\delta(R = 12\ \text{nm}) < 0.10$ while $\delta(R > 100\ \text{nm}) < 10^{-3}$. Clearly the effect (ii) is observable only in the 12-nm sample. This estimate assumes homogeneous alignment along the local cylinder axis. In reality, due to cylinder joints, the configuration is more distorted. For this reason we believe that Eq. (5) underestimates the averaging effect.

(ii) Strong surface anchoring on rough or strongly curved surfaces can substantially reduce the nematic ordering $S(\vec{r})$ in the surface layer. This is realized if the surface induced deformation of the director field is strong on the nematic correlation length scale [45]. However, the AFM observations [see Fig. 1(c)] reveal that the surface of our samples is smooth, ruling out this effect.

(iii) To estimate the importance of defects we assume that the concentration of defects in the sample is roughly given by the concentration of joints of the cylindrical segments. Next we assume that the translational motion of nematic molecules is fast enough so that the average nematic ordering $\langle S \rangle$ is observed. Let us define L_d as the average distance between defects (or joints). Each defect is surrounded by an essentially isotropic core [$S(\text{core}) \approx 0$] of volume $V_{\rm def} \approx 4\pi\xi_n(T)^3/3$ provided that the pore radius is larger than the nematic correlation length $\xi_n(T)$. The average volume of the domain, where S$\approx S_b$, is $V_{\rm dom} \approx \pi R^2 L_d$. The average value of $\langle S \rangle$ within the sample is thus $\langle S \rangle \approx S_b/(1+V_{\rm def}/V_{\rm dom})$. The ensuing line narrowing, assuming a perfect nematic order outside the core and that $S(\vec{r})$ is completely averaged over the distance$\approx L_d$, is

$$\delta(R) \approx 1 - \langle S \rangle / S_b \approx \frac{1}{1 + \frac{4\xi_n^3}{3R^2 L_s}}. \tag{6}$$

In the case $\frac{4\xi_n^3}{3R^2 L_s} < 1$ Eq. (6) simplifies to

$$\delta(R) \approx \frac{4R}{3L_d}\left(\frac{\xi_n}{R}\right)^3. \tag{6'}$$

Deep in the nematic phase $\xi_n \approx a_0 \approx 2$ nm. If the concentration of defects is overestimated by setting $\frac{R}{L_d} = 1$, it follows $\delta(R = 12\ \text{nm}) \approx 0.01$ and that $\delta(R > 100\ \text{nm}) < 10^{-4}$. Thus the contribution of defects is negligible in all cases at least deep in the nematic phase. At the N-I transition the value of the nematic correlation length is anomalously increased [36], $\xi_n(T_{NI}) \approx 20$ nm. In the 150-nm and 200-nm samples the defect contribution is also in this case negligible [$\delta(R > 100\ \text{nm}) < 0.001$]. In contrast, Eq. (5) indicates that in the 12-nm sample the defects have an important role.

This picture is consistent with the measured line splitting $\langle \Delta\nu \rangle$, as well as with the spectrum's $I(\nu)$ temperature evolution (Figs. 2, 3, 4, and 5, respectively). Before discussing the observed line shape it should be kept

in mind that the absorption spectra are only partially motionally averaged. In our case $I(\nu)$ consists of two contributions: (a) a "defect" and (b) a "domain" part. Defects contribute a spectrum with a pronounced central peak. This peak is mostly the consequence of the local averaging over the director field, which strongly changes at the defect site. The existence of the central peak proposed was confirmed in numerical simulations taking into account translational diffusion of molecules in a droplet with the radial director field [18]. The domain part consists of (i) a powderlike or (ii) a fieldlike contribution of curved cylindrical segments (domains) partly averaged by the motional narrowing caused by the distorted director field. The pattern (i) is realized in the case $R/\xi_f \ll 1$ and (ii) for $R/\xi_f \sim 1$ or $R/\xi_f > 1$. This contribution has two pronounced peaks.

The line shape evolution of the 12-nm sample (Fig. 3) is discussed next from the point of view of defects. The field effect contribution is negligible, thus the domain contribution is powderlike. At the transition region the spectrum $I(\nu)$ has a single-peak shape with a pronounced sharp peak at the center, indicating that both the domain and the defect terms contribute. With decreasing temperature the defect contribution decreases and the domain background becomes progressively more pronounced. However, the observed central peak at the transition region can also be the consequence of shifted N-I phase transitions in different domains. Numerical simulations on a similar system [18] suggest that the observed peak is more likely the consequence of this effect.

In larger samples (Figs. 4 and 5) the domain contribution is much larger compared to the defect contribution in the whole temperature interval. In addition, the field effects are pronounced causing substantial deviations from the powderlike pattern. The observed hysteresis phenomena are discussed in the following subsection.

C. Hysteresis

We have shown that the relative strength of the field and elastic contributions is roughly proportional to $(R/\xi_f)^2$. In the 12-, 150-, and 200-nm samples studied we find that $(R/\xi_f)^2 \approx 0.001$, $(R/\xi_f)^2 \approx 0.1$, and $(R/\xi_f)^2 \approx 0.2$, respectively. This means that the field influence is negligible in the 12-nm sample and the elastic and field contributions are comparable in the 150-nm and 200-nm samples. In these samples, the Fréedericksz-like director transition can be induced. In the case that this transition is of first order, hysteresis behavior can be expected [36].

As can be seen from Fig. 4, our experiments confirm this hypothesis. The spectra at the point $[T, B]$ were obtained by following either path a or path b; see Sec. IV. Only in the 150-nm sample were the hysteresis effects observed. This means that in the 200-nm sample the external field is strong enough to overcome the memory effect and in the 12-nm sample the field is too weak to cause significant changes of the nematic director field. The detail analysis of the hysteresis behavior in the 150-nm sample is given below.

In the case where $I(\nu)$ was obtained following path b, the spectrum is almost powderlike. Therefore the isotropic distribution of the director field in the sample is only slightly perturbed by the external field. On the contrary, the line shape $I(\nu)$ obtained by following path a is remarkably different. The outer part of the spectrum, which corresponds to the orientations of $\vec{n}$ closer to $\vec{e}_f$, is enhanced. We shall call the absorption spectrum obtained by following path a "fieldlike" and by following path b "powderlike."

In order to understand this difference we emphasize that in the lowest order the elastic free energy contribution is proportional to S^2, whereas the external field contribution is proportional to S. The free energy can be thus written in a form $F(T) \approx F^{(1)}\langle S(T)\rangle + F^{(2)}\langle S(T)\rangle^2$, where $F^{(1)}$ and $F^{(2)}$ do not depend on S. For the 150-nm sample and $|\vec{B}| \approx 9$ T we find that both terms $F^{(1)}$ and $F^{(2)}$ are comparable in magnitude. This means that in the zero field cooled experiment the elastic free energy contribution is dominant, whereas for a field cooled experiment both contributions are important. In the first case the elastic free energy determines the structure. When an external magnetic field is turned on deep in the nematic phase, the nematic structure is not significantly perturbed. On the other hand, if we cross the N-I phase transition in the presence of an external magnetic field, the nematic structure is determined by both the elastic and magnetic terms in free energy. This means that the line shape of the zero field cooled sample will be powderlike also in the presence of the magnetic field deep in the nematic phase. On the contrary, the line shape of field cooled sample will be fieldlike also deep in the nematic phase.

VI. CONCLUSIONS

We have studied the temperature evolution of the nematic ordering of a 5CB liquid crystal confined to the CPG matrix using deuterium NMR. The SEM and AFM images of our samples indicate that cylindrically shaped pores are strongly interconnected and the surface of the pores is smooth. We studied samples of pore radii 12, 150, and 200 nm.

In the 12-nm sample the behavior of the system is substantially different from the bulk behavior. The N-I transition is gradual and shifted below the bulk T_{NI}. This gradual onset can be caused either by (i) the relatively high concentration of defects that appears at the interconnections of cylindrical pore segments, (ii) the strong local curvature of the pores of the order $\sim \xi_n(T_{NI})$, or (iii) results from the superposition of shifted local discontinuous or gradual domain N-I transitions.

The line shape width in confined samples is always narrower than in the bulk sample. This is mostly due to the motional narrowing, which is effective because of nonhomogeneous nematic director field ordering. This

nonhomogenity is induced by curved cylindrical segments and interconnections between them. In the transition region the inhomogenity in the degree of nematic ordering caused by defects is also important. At lower temperatures the cores of defects are greatly reduced and consequently their influence becomes negligible. Thus, in the transition regime the interconnectedness of pore segments plays an important role. At lower temperatures the single pore characteristics prevail.

In contrast, the line shape temperature evolution reveals that the N-I transition is bulklike in the 150- and 200-nm samples. The transition temperature shift from the bulk value T_{NI} and the influence of defects are negligible.

In the 150-nm sample the ratio $\xi/R \approx 0.1$ indicates a regime where the Fréedericksz-like director field transitions can be induced. The observed hysteresis in the $[T, B]$ plane confirms this assumption. In other samples the hysteresis effects were not observed. The field influence is negligible in the 12-nm sample and is too strong to cause memory effects in the 200-nm sample.

Most of our conclusions are based on the assumption of an axial director field structure within cylindrical segments perturbed by defects at their interconnections. This structure is most plausible in the case of planar anchoring and weak external field influence. The latter influence is negligible in the 12-nm sample where most of the apparent departures from bulk behavior are observed. Note that in this sample the proposed director field between joints most probably exists also in the case of different anchoring conditions. Namely, investigations of director patterns in a similar system [8,31] (a nematic liquid crystal confined to an infinite cylinder with homeotropic boundary conditions) reveals that in the case of weak anchoring (i.e., $R/d_e < 1$) the director field aligns along the cylinder axis despite an antagonistic anchoring tendency. For reasonable anchoring strengths ($W_0 < 510^{-4}$ J/m^2) the ratio R/d_e is always less than one in the 12-nm sample.

In our calculations we assumed uniaxial director field. In the case of a strongly distorted director field, biaxiality can appear. Theoretical studies [46,47] have shown that the core of dislocations is expected to be biaxial with a finite but strongly supressed degree of nematic ordering. Because the core of the biaxial defect is larger than that of the uniaxial one, the average degree of nematic ordering within the core is similar in both cases. In addition, the nematic orientational patterns surronding both defects are qualitatively similar. On this basis we anticipate that taking into account biaxiality would not apparently change the observed spectra because the contributions to $I(\nu)$ are averaged over a volume of linear dimension d_D. This distance is in general larger than the core size of a defect. Thus the details of the defect structure are not important. A more detailed analysis of the effect of biaxiality on the absorption spectra is planned to be the aim of our future investigation.

Since there have been many studies investigating the behavior of liquid crystals confined to various porous materials it is interesting to stress the main qualitative differences in the behavior of such systems. This introduces a certain kind of a classification. As liquid crystal host matrices [11], the aerogels, Vycor glass, CPG, and Nuclepore and Anopore membranes are most commonly used. The Anopore membranes consist of arrays of cylindrical capillarities of relatively narrow distribution of cylinder radia. In this case the single regular pore (SRP) characteristics are dominant. Here "regular" refers to the well defined geometry of the pore. Similar characteristics have Nuclepore membranes, except that the distribution of cylinder radii is broader. The behavior of the system can be described as a superposition of SRP contributions (SSRP behavior) whose eventual differences mainly arise due to different values of the radii. Our study indicates that the behavior of liquid crystals immersed in the CPG porous glass matrix is predominantly SRP far from the N-I transition. In contrast, at the transition the "inter-regular-pore" (IRP) effects are important. A similar system represents Vycor glass with the exception that individual pore segments exhibit larger departures from the cylindrical geometry. Thus liquid crystals immersed into the Vycor glass exhibit SSRP-like behavior deep in the nematic phase. Depending on the concentration of defects IRP behavior could be important at the N-I transition. The most open pore systems represent aerogels that can be described as a structure consisting of strongly interconnected strands. The voids of the irregular shape are in this case strongly interconnected. In this case the "inter-irregular-pore" behavior can be pronounced.

[1] P. G. de Gennes, Science **265**, 495 (1992).
[2] S. Candau, P. LeRoy, and F. Debeauvais, Mol. Cryst. Liq. Cryst. **23**, 283 (1973).
[3] J. W. Doane, N. A. Vaz, B. G. Wu, and S. Žumer, Appl. Phys. Lett. **48**, 269 (1986).
[4] A. Golemme, S. Žumer, D. W. Allender, and J. W. Doane, Phys. Rev. Lett. **61**, 2937 (1988).
[5] H. S. Kitzerov, Liq. Cryst. 16, **1** (1994), and references therein.
[6] P. E. Cladis and M. Kleman, J. Phys. **33**, 591 (1972).
[7] R. B. Meyer, Philos. Mag. **27**, 405 (1973).
[8] D. W. Allender, G. P. Crawford, and J. W. Doane, Phys. Rev. Lett. **67**, 1442 (1991); G. P. Crawford, D. W. Allender, and J. W. Doane, Phys. Rev. A **45**, 8693 (1992).
[9] G. S. Iannacchione and D. Finotello, Phys. Rev. E **50**, 4780 (1994).
[10] S. Kralj and S. Žumer, Phys. Rev. E **51**, 366 (1995), and references therein.
[11] *Liquid Crystals in Complex Geometries Formed by Polymer and Porous Networks*, edited by G. P. Crawford and S. Žumer (Taylor and Francis, London, in press).
[12] M. D. Dadmun and M. Muthukumar, J. Chem. Phys. **98**, 4850 (1993).
[13] G. S. Iannacchione, G. P. Crawford, S. Žumer, J. W.

Doane, and D. Finotello, Phys. Rev. Lett. **71**, 2595 (1993).
[14] G. S. Iannacchione, G. P. Crawford, S. Qian, J. W. Doane, D. Finotello, and S. Žumer, Phys. Rev. E (to be published).
[15] T. Bellini, N. A. Clark, C. D. Muzny, L. Wu, C. W. Garland, D. W. Schaefer, and B. Olivier, Phys. Rev. Lett. **69**, 788 (1992).
[16] N. A. Clark, T. Bellini, R. M. Malzbender, B. N. Thomas, A. G. Rappaport, C. D. Muzny, D. W. Schaefer, and L. Hrubesh, Phys. Rev. Lett. **71**, 3505 (1993).
[17] L. Wu, B. Zhou, C. W. Garland, T. Bellini, and D. W. Schaefer, Phys. Rev. E **51**, 2157 (1995).
[18] S. Kralj, G. Lahajnar, A. Zidanšek, N. Vrbančič-Kopač, M. Vilfan, R. Blinc, and M. Kosec, Phys. Rev. E **48**, 340 (1993).
[19] A. Zidanšek, S. Kralj, G. Lahajnar, and R. Blinc, Phys. Rev. E **51**, 3332 (1995).
[20] X. Wu, W. I. Goldburg, and M. X. Liu, Phys. Rev. Lett. **69**, 470 (1992).
[21] F. M. Aliev and M. N. Breganov, Zh. Eksp. Teor. Fiz. **95**, 122 (1989) [Sov. Phys. JETP **68**, 70 (1989)].
[22] A. Mertelj and M. Čopič (unpublished).
[23] G. Schwalb and F. W. Deeg, Phys. Rev. Lett. **74**, 1383 (1995).
[24] D. J. Cleaver, S. Kralj, T. J. Sluckin, and M. P. Allen, in *Liquid Crystals in Complex Geometries Formed by Polymer and Porous Networks* (Ref. [11]).
[25] A. Maritan, M. Ciepak, T. Bellini, and R. Banavar, Phys. Rev. Lett. **72**, 4113 (1994).
[26] E. B. Priestley, P. J. Wojtowitz, and P. Sheng, *Introduction to Liquid Crystals* (Plenum, New York, 1974), p. 143.
[27] B. Jerome, Rep. Prog. Phys. **54**, 351 (1991), and references therein.
[28] A. Poniewierski and T. J. Sluckin, Liq. Cryst. **2**, 281 (1987).
[29] A. Rapini and M. Papoular, J. Phys. (Paris) Colloq. **30**, C4-54 (1969).
[30] P. Sheng, Phys. Rev. A **26**, 1610 (1982).
[31] S. Kralj and S. Žumer, Phys. Rev. E. **51**, 366 (1995).
[32] D. Monselesan and H. R. Trebin, Phys. Status Solidi **155**, 349 (1989).
[33] J. Nehring and A. Saupe, J. Chem. Phys. **54**, 337 (1971); **56**, 5527 (1972).
[34] P. I. C. Teixeira, V. M. Pergamenshchik, and T. J. Sluckin, Mol. Phys. **80**, 1338 (1993).
[35] A. I. Alexe-Ionescu, G. Barbero, and G. Durand, J. Phys. (France) II **3**, 1247 (1993).
[36] P. G. de Gennes and J. Prost, *The Physics of Liquid Crystals* (Oxford University Press, Oxford, 1993).
[37] A. Abragam, *The Principles of Nuclear Magnetism* (Clarendon, Oxford, 1962).
[38] S. Žumer, S. Kralj, and M. Vilfan, J. Chem. Phys. **91**, 6411 (1989).
[39] G. P. Crawford, R. Stannarius, and J. W. Doane, Phys. Rev. A **44**, 2558 (1991).
[40] G. P. Crawford, R. O. Crawford, S. Žumer, and J. W. Doane, Phys. Rev. Lett. **70**, 1838 (1993).
[41] M. Kléman, *Points, Lines and Walls* (Wiley, Chichester, 1983).
[42] S. Kralj, S. Žumer, and D. W. Allender, Phys. Rev. A **43**, 2943 (1991).
[43] I. Vilfan, M. Vilfan, and S. Žumer, Phys. Rev. A **40**, 4724 (1989).
[44] H. Yokoyama, J. Chem. Soc. Faraday Trans. II **84**, 1023 (1988).
[45] G. Barbero, E. Miraldi, and A. Stepanescu, J. Appl. Phys. **68**, 2063 (1990).
[46] N. Schopohl and T. J. Sluckin, Phys. Rev. Lett. **59**, 2582 (1987).
[47] E. Penzenstadler and H. R. Trebin, J. Phys. (Paris) **50**, 1027 (1989).

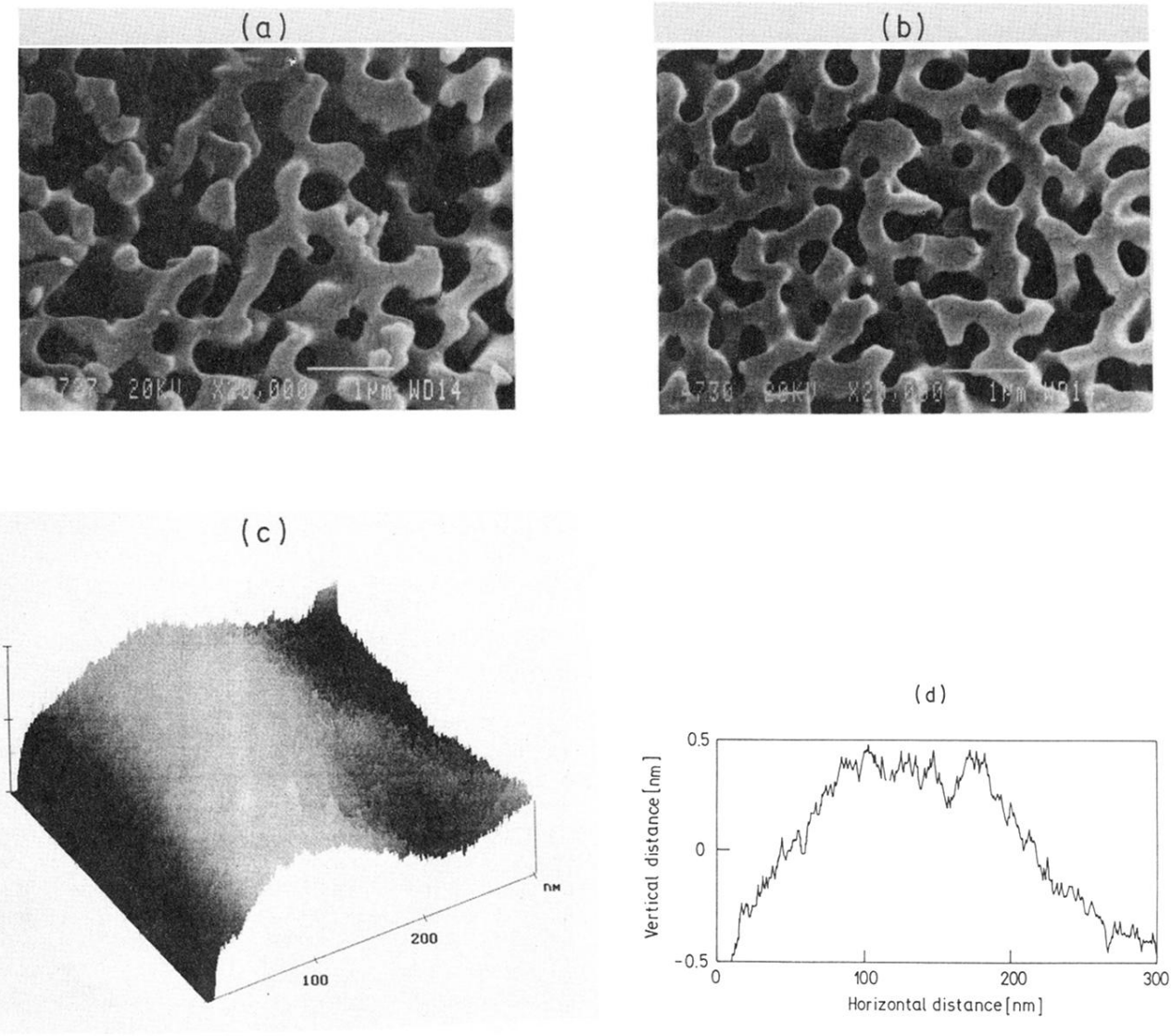

FIG. 1. (a) and (b) SEM and (c) and (d) AFM images. The CPG samples with pore radii (a) $R \approx 200$ nm and (b) $R \approx 150$ nm are shown. Note that in all cases the outer surface of the CPG matrices was probed. The 3D AFM image of the CPG ($R \approx 150$ nm) surface is presented in (c) and the surface profile is shown in (d).